PART III

SENSORS

Magnetic Actuators and Sensors, Second Edition. John R. Brauer.

CHAPTER 10

Hall Effect and Magnetoresistive Sensors

As mentioned in Chapter 1, magnetic sensors use magnetic fields to sense motion. Input energy in the form of mechanical energy and/or electromagnetic energy is converted to electrical energy, and thus magnetic sensors are a type of transducer. Usually magnetic sensors output a signal voltage along with little or no current. The magnetic fields sensed may vary over an extremely broad range as shown in Figure 10.1.

Magnetic sensors using the Hall effect are very common, small, and inexpensive. This chapter examines the behavior, accuracy, and construction of typical Hall sensors. Along with the Hall effect, this chapter also investigates a related parameter called *magnetoresistance*. Note that Figure 10.1 shows that Hall and magnetoresistive (MR) sensors may sense fields as low as approximately 1.E–5 T, and related giant magnetoresistance (GMR) sensors can sense even smaller magnetic fields. While the previous chapters have shown that magnetic actuators usually operate in the range of 1–2 T, magnetic sensors often operate over a much greater range of flux densities.

10.1 SIMPLE HALL VOLTAGE EQUATION

The Hall effect was discovered in 1879 by E. H. Hall. He found that a voltage is developed across a current-carrying semiconductor in a direction normal to the current flow and proportional to the magnetic flux density that is normal to both the current and the voltage difference. The Hall voltage across terminals spaced in the y direction is:

$$V_y = k_H B_z J_x d_y \tag{10.1}$$

where d_y is the terminal (electrode) spacing shown in Figure 10.2, which also shows the current density J_x flowing in the x direction, along with the flux density B_z. The Hall voltage is developed because the current experiences the Lorentz force of

Magnetic Actuators and Sensors, Second Edition. John R. Brauer.

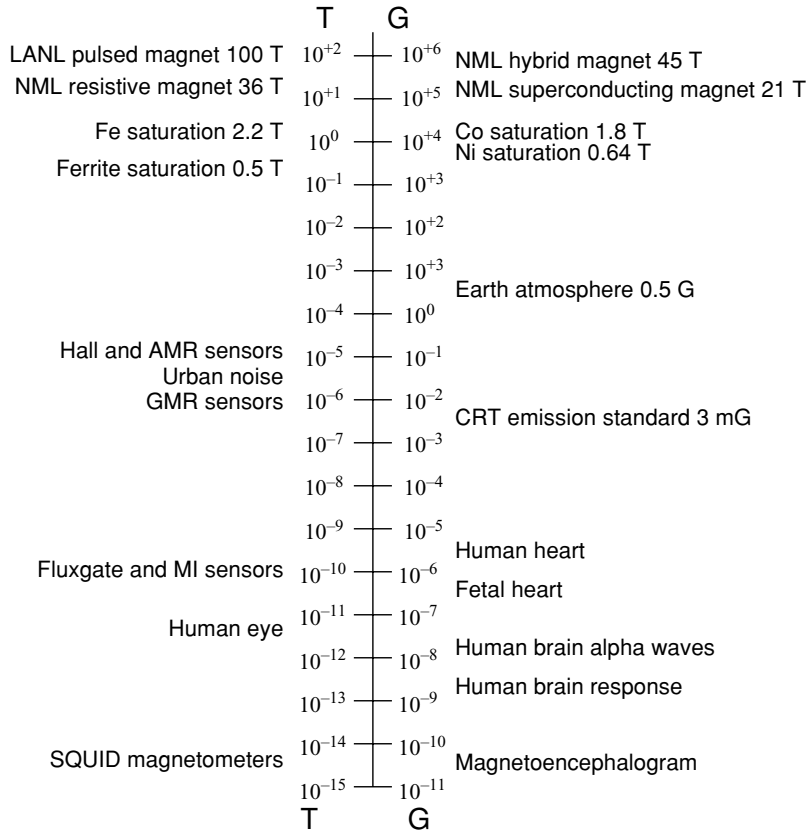

FIGURE 10.1 Range of magnetic flux densities in teslas (T) and gauss (G). The highest values are produced in magnets made by Los Alamos National Laboratory (LANL) or the National Magnet Lab (NML), which have coils that are either superconducting, resistive (using conventional Cu or Al wire), or hybrid (both coil types).

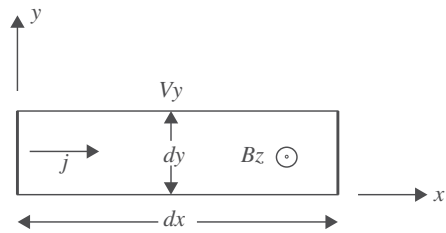

FIGURE 10.2 Hall effect voltage in a narrow semiconductor bar.

Chapter 2. It can be shown that the Hall electric field **E** in volts per meter balances the motional electric field of (2.36) [1].

The Hall coefficient k_H in (10.1) can be shown for a narrow bar with $d_x \gg d_y$ to equal approximately [1]:

$$k_H = -\frac{1}{ne} \tag{10.2}$$

where n is the electron concentration in electrons per cubic meter and e is the charge on an electron = 1.602E–19 C. The electron concentration varies with the semiconductor material used. Typically, silicon is used, because it is so widely available, thermally stable, inexpensive, and has conductivity in the semiconductor range. In fact, many Hall sensors are built within CMOS or other integrated silicon circuits. The semiconductor range of conductivity is within several orders of magnitude of 1 S/m, and can be varied by doping with impurities. If doped so as to contain holes, the Hall constant of (10.2) becomes:

$$k_H = \frac{1}{pe} \tag{10.3}$$

where p is the hole concentration in holes per cubic meter.

Practical Hall sensors often have many large electrodes and a wide range of geometries, which can make the accuracy of (10.1) poor. To analyze a wide range of geometries and materials, a numerical technique is required that will solve for current flow in Hall sensors [2].

10.2 HALL EFFECT CONDUCTIVITY TENSOR

Current flow is governed by Ohm's law for fields given in Chapter 2. When conductivity σ is anisotropic (dependent on direction), then it must be expressed as a matrix called a tensor, and Ohm's law becomes:

$$\begin{bmatrix} J_x \\ J_y \\ J_z \end{bmatrix} = \begin{pmatrix} \sigma_{xx} & \sigma_{xy} & \sigma_{xz} \\ \sigma_{yx} & \sigma_{yy} & \sigma_{yz} \\ \sigma_{zx} & \sigma_{zy} & \sigma_{zz} \end{pmatrix} \begin{bmatrix} E_x \\ E_y \\ E_z \end{bmatrix} \tag{10.4}$$

Because an applied magnetic field produces a Lorentz force on moving electrons, the above conductivity tensor is indeed anisotropic. Fermi gas theory of free electrons [3] experiencing **B** in the z direction produces the following matrix elements of (10.4):

$$\sigma_{xx} = \sigma_{yy} = \frac{\sigma_o}{1 + (\omega_c \tau)^2} \tag{10.5}$$

$$\sigma_{xy} = \frac{-\omega_c \tau \sigma_o}{1 + (\omega_c \tau)^2} \tag{10.6}$$

$$\sigma_{yx} = \frac{\omega_c \tau \sigma_o}{1 + (\omega_c \tau)^2} \tag{10.7}$$

$$\sigma_{xz} = \sigma_{xz} = \sigma_{xz} = \sigma_{xz} = 0 \tag{10.8}$$

$$\sigma_{zz} = \sigma_o \tag{10.9}$$

where ω_c is the cyclotron frequency for a free electron, τ is the collision time, and σ_o is the *bulk conductivity* [3]:

$$\sigma_o = ne^2\tau/m \tag{10.10}$$

where m is electron mass = 9.1085E–21 kg. The cyclotron frequency of the free electrons due to the force of the magnetic field is:

$$\omega_c = eB/m \tag{10.11}$$

Because (10.6) and (10.7) differ for $B > 0$, Hall effect and magnetoresistance create an *unsymmetric* conductivity tensor.

The Hall voltage equation (10.1) can be derived by making the following assumptions:

(1) Assuming $E_z = 0$, then (10.4)–(10.9) give:

$$J_y = \frac{\sigma_o}{1 + (\omega_c \tau)^2}(\omega_c \tau E_x + E_y) \tag{10.12}$$

(2) Assuming $J_y = 0$, then (10.12) and (10.11) give:

$$E_y = -\omega_c \tau E_x = -\frac{eB}{m} E_x \tag{10.13}$$

Next, (10.4)–(10.9) give:

$$J_x = \frac{\sigma_o}{1 + (\omega_c \tau)^2}(E_x - \omega_c \tau E_y) \tag{10.14}$$

Substituting (10.13) into (10.14) gives:

$$J_x = \sigma_o E_x \tag{10.15}$$

(3) Assuming E_y is uniform in y, then (10.13) gives:

$$V_y = E_y d_y = -d_y \frac{eB_z \tau}{m} E_x \tag{10.16}$$

Substituting (10.15) and then (10.10) obtains the Hall voltage:

$$V_y = -d_y \frac{eB_z\tau}{m\sigma_o} J_x = -d_y \frac{B_z J_x}{ne} \tag{10.17}$$

Note that (10.17) agrees with (10.1) and (10.2). However, the above three assumptions have to hold true for the simple equation (10.1) to apply. These assumptions are valid only for narrow bars with infinitesimal Hall voltage sensing electrodes.

Example 10.1 Simple Hall Equation Applied to Semiconducting Bar A wide bar of semiconductor material as shown in Figure 10.2 has dimensions $8 \times 10 \times 0.25$ mm in *x, y,* and *z,* respectively. The measured current *I* in the *x* direction is 2.5 mA for 1 V applied across the current-carrying electrodes at $x = 0$ and $x = d_x$.

(a) Calculate the bulk resistance and σ_o.
(b) A narrow bar of the same material and current density placed in a magnetic field of 1 T obtains a Hall electric field of −23.8 V/m. Find the Hall coefficient and the conductivity tensor.

Solution

(a) The bulk resistance is $R = V/I = 1/.0025 = 400\ \Omega$. Analogous to reluctance of Chapter 3, resistance of a bar obeys:

$$R = l/(\sigma S) \tag{E10.1.1}$$

where as in Chapter 3, l is length and S is cross-sectional area. Substituting the length and area of the wide bar obtains the bulk conductivity $\sigma_o = 8$ S/m, which is within the wide conductivity range of semiconductors.

(b) From (10.17), (10.1), and (10.2), the Hall electric field for the narrow bar is:

$$E_y = k_H B_z J_x \tag{E10.1.2}$$

In terms of resistivity ρ, the inverse of conductivity, where $1/\sigma_o = 1/8 = 0.125$:

$$\begin{bmatrix} E_x \\ E_y \end{bmatrix} = \begin{pmatrix} 0.125 & -k_H B_z \\ k_H B_z & 0.125 \end{pmatrix} \begin{bmatrix} J_x \\ J_y \end{bmatrix} \tag{E10.1.3}$$

Given the −23.8 V/m measurement for $J_x = I/S = 1000$ A/m^2, the off-diagonal terms can be filled in to give:

$$\begin{bmatrix} E_x \\ E_y \end{bmatrix} = \begin{pmatrix} 0.125 & 0.0238 \\ -0.0238 & 0.125 \end{pmatrix} \begin{bmatrix} J_x \\ J_y \end{bmatrix} \tag{E10.1.4}$$

The Hall coefficient is thus $k_H = -0.0238$. The tensor conductivity is the inverse of the above resistivity tensor matrix:

$$\begin{pmatrix} \sigma_{xx} & \sigma_{xy} \\ \sigma_{yx} & \sigma_{yy} \end{pmatrix} = \begin{pmatrix} \rho_{xx} & \rho_{xy} \\ \rho_{yx} & \rho_{yy} \end{pmatrix}^{-1} \tag{E10.1.5}$$

which means that the product of the resistivity and conductivity tensors is unity:

$$\begin{pmatrix} \rho_{xx} & \rho_{xy} \\ \rho_{yx} & \rho_{yy} \end{pmatrix} \begin{pmatrix} \sigma_{xx} & \sigma_{xy} \\ \sigma_{yx} & \sigma_{yy} \end{pmatrix} = \begin{pmatrix} 1 & 0 \\ 0 & 1 \end{pmatrix} \tag{E10.1.6}$$

The conductivity tensor can be easily found in the case when (10.5)–(10.8) make diagonal terms equal and off-diagonal terms equal but opposite in sign:

$$\begin{pmatrix} \rho_{xx} & \rho_{xy} \\ -\rho_{xy} & \rho_{xx} \end{pmatrix} \begin{pmatrix} \sigma_{xx} & \sigma_{xy} \\ -\sigma_{xy} & \sigma_{xx} \end{pmatrix} = \begin{pmatrix} 1 & 0 \\ 0 & 1 \end{pmatrix} \tag{E10.1.7}$$

Multiplying out the left side and using Cramer's rule gives:

$$\sigma_{xx} = \rho_{xx}/(\rho_{xx}^2 + \rho_{xy}^2) \tag{E10.1.8}$$

$$\sigma_{xy} = -\rho_{xy}/(\rho_{xx}^2 + \rho_{xy}^2) \tag{E10.1.9}$$

which for the resistivity tensor of (E10.1.4) gives the desired conductivity tensor:

$$\begin{pmatrix} \sigma_{xx} & \sigma_{xy} \\ \sigma_{yx} & \sigma_{yy} \end{pmatrix} = \begin{pmatrix} 7.72013 & -1.46991 \\ 1.46991 & 7.72013 \end{pmatrix} \tag{E10.1.10}$$

10.3 FINITE-ELEMENT COMPUTATION OF HALL FIELDS

To predict Hall voltages for arbitrary geometries, including bars that are not narrow, as well as for arbitrary materials, a numerical method is needed. Similar to the finite elements of Chapter 4 for magnetic fields, here finite elements are applied to current flow problems with anisotropic tensor conductivity.

10.3.1 Unsymmetric Matrix Equation

From Ohm's law, voltages and currents are related by the matrix equation:

$$[C]\{V\} = \{I\} \tag{10.18}$$

where $[C]$ is the conductance matrix. Chapter 4 showed that finite elements have shape functions. For a shape function N of any type, it can be shown that the conductance

matrix is of the form:

$$[C] = \sum dv[\nabla N]^T[\sigma][\nabla N] \tag{10.19}$$

where the summation is over volume integrals of individual finite elements. Note that the tensor conductivity appears, postmultiplied by the gradient of N and premultiplied by the matrix transpose of the gradient of N. Because the Hall effect conductivity tensor of (10.4) is unsymmetric, the conductance matrix $[C]$ is also unsymmetric for nonzero magnetic fields. Thus the finite element software used to solve (10.18) must have the capabilities of inputting and solving an unsymmetric matrix.

10.3.2 2D Results

Finite-element software that solves DC current flow problems with unsymmetric conductivity tensors has been used to analyze Hall effect and the related magnetoresistance. Here 2D finite-element analysis is applied to several examples.

Example 10.2 Hall Voltage Computed for Wide 2D Semiconductor Bar of Example 10.1 The wide bar of semiconductor material of Example 10.1 has the conductivity tensor determined in that example. Use the unsymmetric conductivity tensor in 2D finite-element software to compute the actual Hall electric field in the wide bar along with the resistance of the bar.

Solution The results are shown in Figure E10.2.1 and included in Table 10.1. Note that quadrilateral finite elements are used, all squares 1 mm on a side. The voltage contours in Figure E10.2.1a are "S" shaped due to Hall effect, which produces the

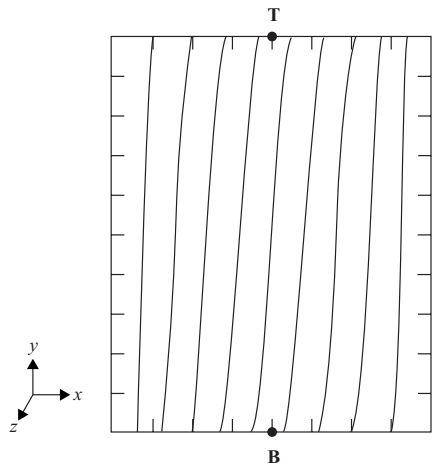

(a)

FIGURE E10.2.1 Finite-element model with 1–mm^2 elements and computed results for Hall sensor of dimensions 8 mm in x and 10 mm in y. **B** is in the z direction and applied **J** in x direction. The top electrode is indicated by T and the bottom electrode is indicated by B. (a) voltage contours, (b) Hall electric field in y direction, (c) current density vectors.

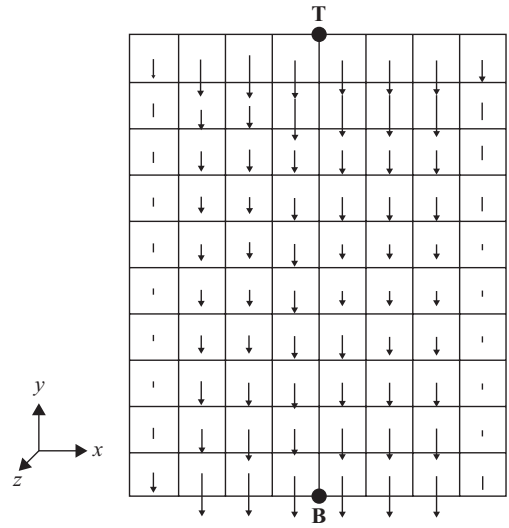

(b)

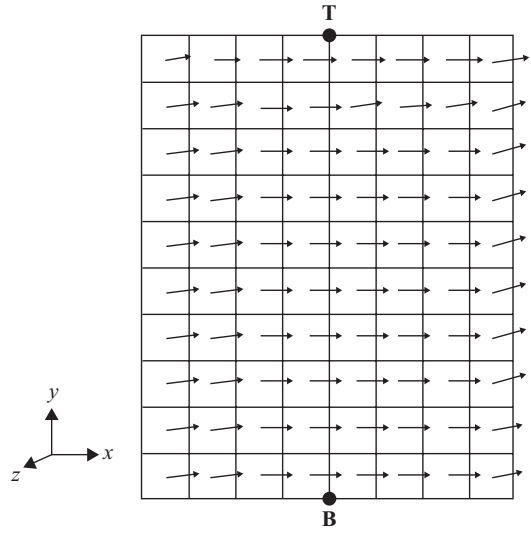

(c)

FIGURE E10.2.1 (*Continued*)

TABLE 10.1 Calculated Hall Fields and Magnetoresistance R_M

Model Dimensions (mm)	A_{el} (mm^2)	V_B (V)	V_T (V)	$E_{y,av}$ (V/m)	R_M (Ω)	R_M (%)
2D 8 × 10 × 0.25	0	0.43304	0.56696	–13.39	408.51	102.13
2D 8 × 2 × 0.25	0	0.47635	0.52365	–23.65	2011.5	100.58
3D 8 × 10 × 2	2	0.44575	0.55425	–10.85	48.978	102.26
3D 8 × 2 × 2	2	0.48489	0.51511	–15.11	187.66	100.98

y components of electric field in Figure E10.2.1b. The current density has both *x* and *y* components as shown in Figure E10.2.1c. The top row of Table 10.1 shows that the actual Hall electric field is –13.39 V/m, considerably reduced from the −23.8 V/m obtained for the narrow rod as described in Example 10.1. Table 10.1 lists the voltage V_T in the top Hall electrode and the voltage V_B in the bottom Hall electrode, whose difference is the Hall voltage. Note also in the top row of Table 10.1 that the resistance is now 408.51 Ω, an increase from the 400 Ω without a magnetic field. The increased resistance is called magnetoresistance.

Example 10.3 Hall Voltage Computed for More Narrow 2D Semiconductor Bar
The semiconductor material with the conductivity tensor of Examples 10.1 and 10.2 is used in a bar of size 8 × 2 × 0.25 mm. Use the unsymmetric conductivity tensor in 2D finite-element software to compute the actual Hall voltage and magnetoresistance.

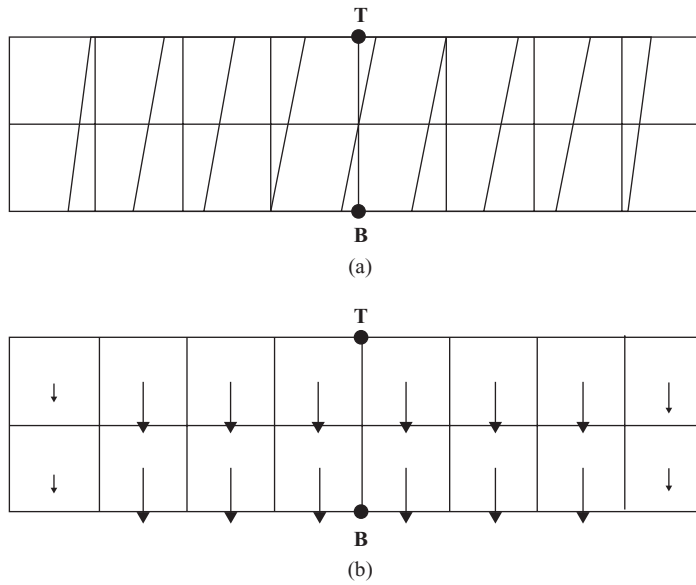

FIGURE E10.3.1 Finite-element model with 1–mm^2 elements and computed results for Hall sensor of dimensions 8 mm in *x* and 2 mm in *y*. **B** is in the *z* direction and applied **J** in the *x* direction. The top electrode is indicated by T and the bottom electrode is indicated by B. (a) voltage contours, (b) Hall electric field in *y* direction.

Solution The results are shown in Figure E10.3.1 and included in Table 10.1. The voltage contours in Figure E10.3.1a are slanted due to Hall effect, which produces the y components of electric field in Figure E10.3.1b. The second row of Table 10.1 shows that the actual Hall electric field is -23.65 V/m, very close to the –23.8 V/m obtained for the narrow rod as described in Example 10.1. Note also in the second row of Table 10.1 that the resistance is now 2011.5 Ω, a small percentage increase from the 2000 Ω without a magnetic field.

Example 10.4 Effect of Finite Hall Electrodes on Current Flow The wide bar of semiconductor material of Example 10.1 is placed where there is no magnetic field. Maxwell is to be used to find its voltage contours and current flow pattern for two cases. The first case has no Hall electrodes. The second case has two Hall aluminum electrodes of size 1 mm in x and 1 mm in y. In both cases the applied magnetic field is assumed to be zero, and the power loss is also to be found.

Solution First, change the Solver in Maxwell to "DC Conduction." Next, enter the 8×10-mm rectangular box for the geometry, and also use boxes for both electrodes. Under "Setup Materials," since there is no magnetic field, the bulk conductivity of 8 S/m is entered. The electrodes are first made the same 8 S/m, and later changed to aluminum. Finally, boundary conditions of 1 V on the left edge and 0 V on the right edge are specified.

The computed voltage contours without aluminum electrodes are shown in Figure E10.4.1a, and the computed current density arrows are in Figure E10.4.1b. The

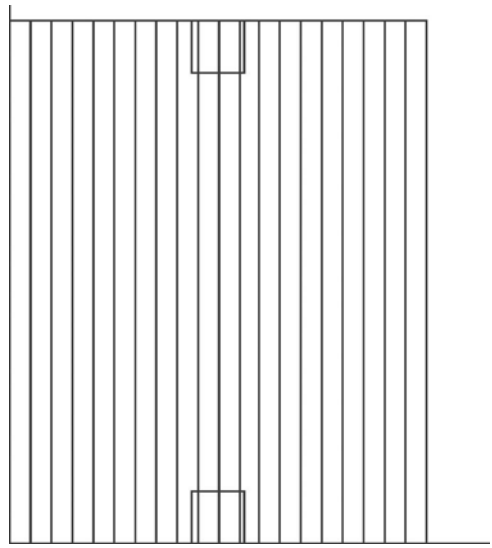

(a)

FIGURE E10.4.1 Wide semiconductor bar of Example 10.4 with no applied magnetic field. (a) computed voltage contours, (b) computed current density arrows.

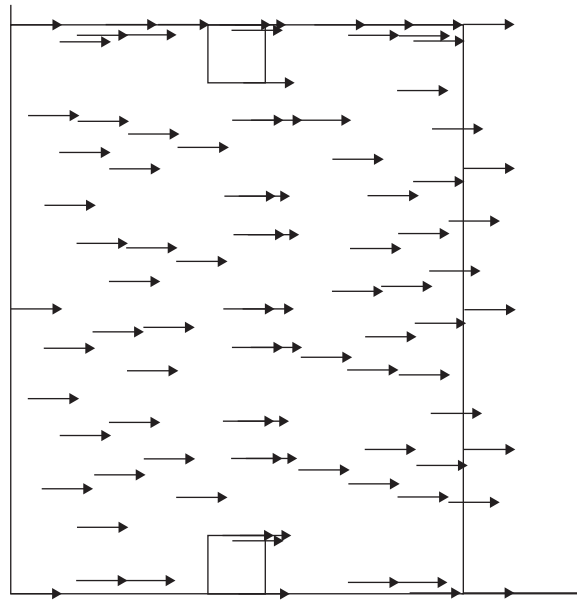

(b)

FIGURE E10.4.1 (*Continued*)

computed power loss is exactly 10 W for 1 m depth. Since for 1 m depth the resistance from (E10.1.1) is 0.1 Ω, the expected power loss is $V^2/0.1 = 10$ W, agreeing with the computed power loss.

The computed voltage contours with aluminum electrodes are shown in Figure E10.4.2a, and the computed current density arrows are in Figure E10.4.2b. Both patterns show that the aluminum electrodes perturb the field. The computed power loss is now 10.7365 W for 1 m depth. The power loss has increased for 1 V because some of the semiconductor is replaced by aluminum, reducing the resistance.

10.3.3 3D Results

To compute the voltage contours, Hall electric field and voltage, and resistance of sensors with 3D geometries, 3D finite elements are used to assemble the matrix equation of (10.18). The shape function of (10.19) for the first-order 3D finite elements used here obtains a voltage within an element obeying:

$$V(x, y, z) = \sum_{k=L,M,N,O} V_k(1 - a_k x)(1 - b_k y)(1 - c_k z) \tag{10.20}$$

Thus the shape function of (10.19) is:

$$N = (1 - a_k x)(1 - b_k y)(1 - c_k z) \tag{10.21}$$

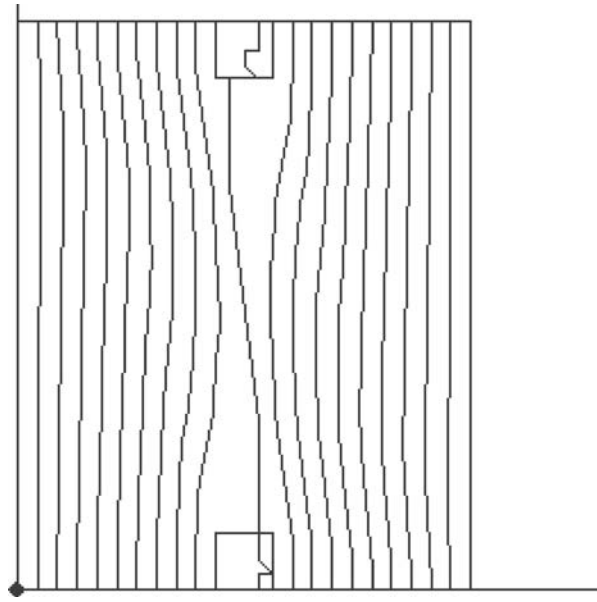

(a)

(b)

FIGURE E10.4.2 Computer display of wide semiconductor bar of Example 10.4 with no applied field but with 1 × 1-mm aluminum electrodes. (a) computed voltage contours, (b) computed current density arrows.

The 3D finite elements in the examples below are all hexahedrons, which are six-sided solids. In the examples below the hexahedrons are all cubes, but they could be any shape not distorted greatly from a rectangular box. Other 3D finite elements include the tetrahedrons discussed in Chapter 4.

Example 10.5 Hall Voltage Computed for Wide 3D Semiconductor Bar with Finite Hall Electrodes The wide bar of semiconductor material of Example 10.1 has the conductivity tensor determined in that example. The Hall electrodes are thin highly conducting plates of area 2×1 mm as shown in Figure 10.1, which shows a bar thickness of 2 mm. Use the unsymmetric conductivity tensor in 3D finite-element software to compute the actual Hall voltage contours and electric field in the wide bar along with the resistance of the bar.

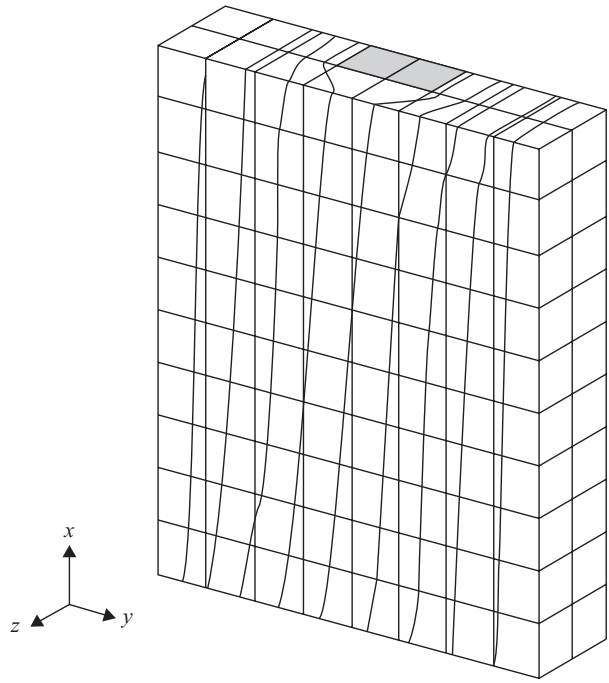

FIGURE 10.1 Finite-element model with 1–mm^3 elements and computed voltage contours for Hall sensor of dimensions $8 \times 10 \times 2$ mm.

Solution The computed voltage contours are shown in Figure 10.1, in which the electrodes were assumed to be perfectly conducting. Other computed results are listed in row 3 of Table 10.1. Notice that the Hall electrodes and other 3D effects have reduced the Hall electric field to -10.85 V/m, even further from the predicted -23.8 V/m of (10.1).

Example 10.6 Hall Voltage Computed for Narrower 3D Semiconductor Bar with Finite Hall Electrodes The narrower bar of semiconductor material of Example 10.2 is made 2 mm thick in the third (z) dimension. It has thin highly conducting plates of area 2×1 mm for Hall electrodes, as shown in Figure E10.6.1. Use the unsymmetric conductivity tensor in 3D finite-element software to compute the actual Hall voltage contours and electric field in the narrower bar along with the resistance of the bar.

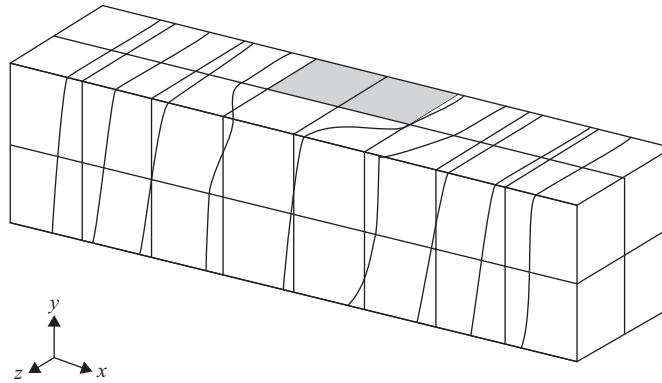

FIGURE E10.6.1 Finite-element model with 1–mm^3 elements and computed voltage contours for Hall sensor of dimensions $8 \times 2 \times 2$ mm.

Solution The computed voltage contours are shown in Figure E10.6.1, in which the electrodes were assumed to be perfectly conducting. Other computed results are listed in row 4 of Table 10.1. Notice that the Hall electrodes and other 3D effects have reduced the Hall electric field to -15.11 V/m, much further from the predicted -23.8 V/m of (10.1) than the -23.65 V/m of the 2D case.

10.4 HALL SENSORS FOR POSITION OR CURRENT

10.4.1 Toothed Wheel Position Sensor

The Hall sensor element can be used in a magnetic circuit to sense position. The most popular magnetic circuit has the toothed wheel, which may be a gear, shown in Figure 10.3. The sensor of Figure 10.3 is commonly used in the automotive industry for wheel position and speed sensing. Four wheel sensing is essential for the following automotive safety systems.

- Anti-lock braking, in which zero or low speed of one or two wheels indicates sliding on ice etc. and therefore triggers rapid pumping actuation of the brakes.
- Traction control, in which high speed of one or two wheels indicates spinning on ice etc. and therefore triggers changes in engine torque applied to the wheels.

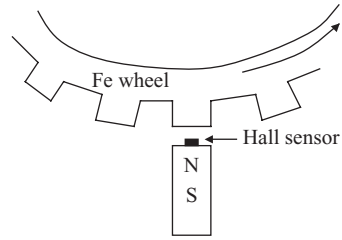

FIGURE 10.3 Toothed wheel position sensor with Hall effect magnetic field detector mounted on a permanent magnet with N and S poles.

- Brake force distribution, in which higher speed of certain wheels carrying a heavier cargo load indicates that they need greater braking force.
- Stability control, in which zero or low speed of one or two wheels during turning indicates a side skid and therefore triggers changes in engine torque applied to the wheels.

In most of the above systems, feedback control as shown in Figure 1.4 is used with both the magnetic sensor and an actuator. The actuator may be purely magnetic or may also involve an electrohydraulic system to be discussed in Chapter 16.

In Figure 10.3 the magnetic field is supplied by a permanent magnet stator. In some cases, a coil winding on a steel stator can be used instead, as analyzed in Example 3.2. As described in Example 3.2, the reluctance changes as the steel wheel teeth rotate past the stator. This variable reluctance causes the magnetic flux and flux density to change. For simplicity, assume the Hall sensor is subjected to a sinusoidal B change with wheel angular position θ of the type:

$$B(\theta) = B_{pk} \sin n_T \theta \tag{10.22}$$

where n_T is the number of teeth on the wheel.

Assume also that the above flux density is in the z direction of Figure 10.2 and (10.1), which applies along with a current density J_x and Hall sensor dimension d_y. Then (10.22) and (10.1) give the sensor output voltage:

$$V_y = k_H J_x d_y B_{pk} \sin n_T \theta \tag{10.23}$$

Because the above four coefficients are all constants, the sensor output voltage is directly proportional to $\sin(n_T\theta)$. Thus the position θ is sensed over a tooth "pitch", and speed is also easily sensed by taking the time derivative of the output voltage.

In actuality, the simple sinusoid assumed in (10.22) is only an approximation. Finite-element analysis can determine the exact variation with position for any tooth shape. To sense absolute position, a particular tooth can be removed or the tooth pattern can be made nonuniform.

Example 10.7 Hall Sensor Output for Toothed Wheel of Example 3.2 A small Hall sensor is inserted in the airgap between the teeth of Example 3.2. Assume that the Hall sensor is supplied a current and is arranged as in Figure 10.2 to sense the magnetic flux density, which is assumed to vary sinusoidally between the values of Example 3.2. Find the expression for the output voltage as a function of position.

Solution From Example 3.2, the flux density varies from 0.06285 T to 0.6285 T. Assuming a sinusoidal variation gives:

$$B(\theta) = 0.06285 + (0.6285 - 0.06285)\sin n_T\theta \tag{E10.7.1}$$

Substituting in (10.1) gives the output voltage:

$$V_y = k_H J_x d_y (0.06285 + 0.5656 \sin n_T\theta) \tag{E10.7.2}$$

where the three coefficients are all constants.

10.4.2 Position Sensors using Multipole Magnets

Instead of a toothed wheel, position sensors can be made using Hall sensor elements placed near moving multipole permanent magnets [4]. Sensors have been made for position range as great as 5 m. The magnets can be made of flexible thin material that is glued to the moving surface. In this way one makes an *encoder*, a sensor that determines position. Figure 10.4 shows typical encoders using multipole permanent magnets.

Besides encoders for linear position sensing, even more popular are encoders for sensing rotary position, that is, shaft angle. Multiple permanent magnets are mounted on the shaft, and then a nearby Hall element or elements are used to make a rotary encoder. This encoder can then be used to control commutation of rotary motors such as brushless DC motors [5]. Since such motors usually have a permanent magnet rotor, sometimes no additional permanent magnets are needed.

10.4.3 Hall Effect Current Sensors

Since Ampere's law states that magnetic intensity is proportional to current, Hall magnetic field sensors can be used to sense current. With the aim of reducing currents

FIGURE 10.4 Multipole permanent magnets for linear position and rotary position encoders, with rectangular Hall sensors vertically separated by typically less than 15 mm [4].

and associated power loss, it is increasingly desirable to use current sensors as meters throughout circuits used in industrial plants.

An advantage of Hall sensors for current metering is that isolation from voltages is inherent thanks to their magnetic coupling [6]. Each Hall sensor should be aligned with the expected direction of the magnetic field, which is circumferential for a current-carrying wire as shown in Figure 2.4. If two nearby wires carrying opposite but equal currents replace the one wire in Figure 2.4, then the Hall sensor can be used to make a ground-fault circuit interrupter; the field sensed becomes large only if the current in one wire flows elsewhere through a human or an animal. Instead of Hall sensors, other magnetic field sensors including magnetoresistive sensors may be used to meter current [7], including Chattock coils as will be presented in the next chapter.

10.5 MAGNETORESISTANCE

Both Hall effect and related magnetoresistance are extremely popular methods of sensing magnetic fields. In the past few years devices using magnetoresistance, commonly abbreviated MR, have become ever more popular as new forms of MR are developed. The basic definition of magnetoresistance is the change in resistance due to application of a magnetic field.

10.5.1 Classical Magnetoresistance

Sections 10.1–10.3 have shown that magnetic fields acting on semiconductors produce both Hall effect and magnetoresistance. This type of magnetoresistance is shown in Table 10.1 to be in the range of a 1–10% change. This type of "classical" magnetoresistance is commonly called AMR, for anisotropic magnetoresistance, since its conductivity in (10.4) is anisotropic.

Since the same semiconducting material produces both Hall effect and magnetoresistance, either can be used to make a sensor. Since the magnetoresistance changes of Table 10.1 classical AMR are only a few percent, many engineers prefer to use the Hall voltage, even though it requires addition of the two Hall electrodes.

10.5.2 Giant Magnetoresistance

In 1988 a much larger percentage change in magnetoresistance was discovered and appropriately named *giant magnetoresistance (GMR)*. Throughout the 1990s, GMR was developed extensively, especially for sensing magnetic fields recorded on computer disk drives, magnetic stripes on credit cards, and so on [8, 9]. In 2007 the discoverers of GMR, Albert Fert and Peter Grünberg, shared the Nobel Prize in physics.

GMR is very different from classical MR. It requires a multilayer structure of very thin films. It attains change in resistance as high as 65% due to the change in magnetization of the successive magnetic layers. For example, layers of Fe can be coupled antiferromagnetically (with opposite electron spins [3]) through nonmagnetic

Cr layers. When the magnetic field to be sensed is applied, the antiferromagnetic coupling can be overcome, making the magnetic layers parallel. The resistance varies as the cosine of the angle between the magnetizations. Thus the resistance in the antiparallel (AP) case is much greater than the resistance in the parallel case.

There are several different designs for GMR sensors. One sensor has two ferromagnetic (FM) layers sandwiching the GMR material. The two layers are often called *soft adjacent layers* (SALs). Often one of the layers has fixed magnetization, while the other is varied by the field to be sensed. Maximum current (minimum resistance) occurs when the two layers have parallel magnetism.

GMR is now very commonplace for read heads for hard disk computer drives. A later development to increase storage density is called CPP-GMR [10, 11]. CPP stands for current perpendicular to plane, in contrast with the present CIP-GMR, where CIP stands for current in plane. The last section of this chapter will discuss a recent type of GMR sensor called a spin valve sensor.

10.5.3 Newer Forms of Magnetoresistance

There are additional forms of magnetoresistance. All are being investigated to possibly replace GMR in the near future.

- *Tunneling Magnetoresistance (TMR).* Again placed between two SALs, the material used here is a very thin insulator carrying current by quantum tunneling of electrons when subjected to a magnetic field. This tunneling effect was first observed in 1975 but is presently being developed to possibly replace GMR for disk drive read heads. A TMR of 8% was achieved in 2011 using a magnetic tunnel junction sensor [12] for magnetic nanoparticles of the type discussed in Example 7.7. Quantum mechanical effects such as tunneling are mostly beyond the scope of this book.
- *Colosal Magnetoresistance (CMR).* Insulating manganese oxide crystals are changed from nonmagnetic insulators to FM conductors by the magnetic field to be sensed. However, such a change requires very low temperatures and a field greater than 1 T. Thus CMR is not very promising at the present time.
- *Extraordinary Magnetoresistance (EMR).* This more recent form of MR is based upon classical MR, but adds conducting particles to the semiconducting material. As shown in Example 10.4, adding highly conducting materials alters the electric field and current flow patterns. In EMR, many conducting particles are placed inside the semiconductor, thus causing concentrations in the current density. The percentage change in resistance can exceed 35% [13–15].

10.6 MAGNETORESISTIVE HEADS FOR HARD DISK DRIVES

As explained above, MR material is commonly placed near an SAL. In the head of Figure 10.5, an MR layer called a *stripe* is separated from an SAL by a thin nonmagnetic spacer. The applied current in the MR stripe is in the direction out of the

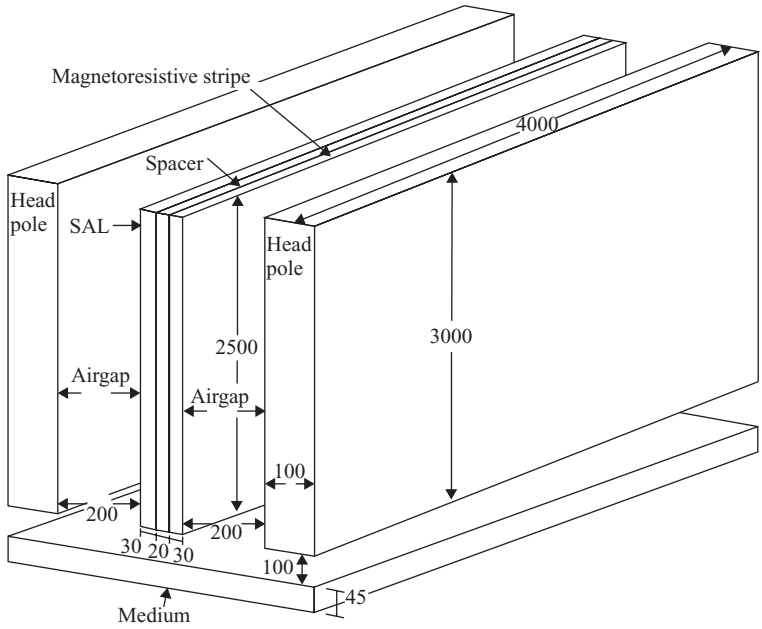

FIGURE 10.5 Geometry of typical magnetoresistive head. Dimensions in nanometers are typical of the 1990s and have since been reduced. The applied current flows out of the page.

page. The nanometer dimensions of Figure 10.5 are typical of MR heads of the mid 1990s [16]. While small, nowadays MR heads are even smaller, making them true examples of nanotechnology and microelectromechanical systems (MEMS) [17].

The head shown in Figure 10.5 is used to sense, that is, to read the magnetic bits previously recorded on the disk medium. The highly permeable head poles direct some of the flux from the disk to the MR stripe. The magnetized medium typically has a B–H curve with a slope of two or three times the permeability of air and a residual flux density B_r of approximately 0.5 T.

Assuming the MR stripe exhibits classical MR, the anisotropic conductivity of (10.4)–(10.9) has been used in 3D finite-element software [16]. The computed MR due to the magnetized media was 2.1%, and the computed voltage contours have the slant of the type shown in Figure E10.6.1.

10.7 GIANT MAGNETORESISTIVE SPIN VALVE SENSORS

GMR introduced in Section 10.5 has led to the development of *spin valve sensors*. They contain two FM layers separated by a normal metal (NM) layer. The magnetization of one FM layer is fixed, while the magnetization of the other FM layer can rotate in response to the external magnetic field that is being sensed.

As mentioned in Chapter 2, magnetization is caused by electron motion. There are two kinds of electron motion [18]. *Orbital* electron motion (along orbits such as

planets orbiting the sun) can be likened to current flowing in a loop, thereby creating magnetic fields according to Ampere's law. *Spin* of electrons was postulated in 1925 to explain certain magnetic observations and later was explained theoretically using quantum mechanics. The electron can be approximated as a sphere with charge on its surface; if this sphere (or other 3D shape) rotates or spins, the resulting current creates a magnetic field. The direction of this spin magnetic field reverses if the spin reverses. According to the Pauli exclusion principle, each energy level in an atom contains a maximum of two electrons, and they must have opposite spins.

Spin valves operate using the two spin states of the FM material, which is here assumed to be cobalt (Co) [19] but could also be a compound of iron and cobalt. In the two-current model, the two spin directions along a fixed quantization axis are up (denoted by $\uparrow$) and down (denoted by $\downarrow$) and are assumed independent of each other. In Co, the two spin states are shifted in energy with density of states (DOS, the energy per unit range of energy) of $\downarrow$ electrons larger than the DOS of $\uparrow$ electrons. The differences in DOS at the Fermi energy level (a typical electron energy) between the two spin types contributes to a spin-asymmetry in the transport properties of the FM. The smaller DOS of the $\uparrow$ electrons reduces their relaxation rate and thus they have a much larger conductivity than the $\downarrow$ electrons. Thus if a small voltage is applied across the FM layer most of the current will be carried by the $\uparrow$ electrons; the current is said to have spin polarization.

The in-plane resistance of a system of NM layers sandwiched between FM layers is examined as follows. Assume the magnetization in consecutive FM layers is parallel (P) and AP (antiparallel) to the spin quantization axis. Assuming no spin-flip scattering, the two spin types are independent parallel conducting channels, and their conductances (reciprocals of resistances) simply add as in a simple DC electric circuit. Denoting the resistances as $R_\uparrow$ and $R_\downarrow$, the total parallel resistance (for the P layer) from circuit theory is the product over the sum:

$$R_P = R_\uparrow R_\downarrow / (R_\uparrow + R_\downarrow) \tag{10.24}$$

In the AP case, the two spin layers each have the same resistance $\frac{1}{2}(R_\uparrow + R_\downarrow)$, giving the total AP resistance:

$$R_{\mathrm{AP}} = (R_\uparrow + R_\downarrow)/4 \tag{10.25}$$

The GMR ratio factor is thus:

$$F_{\mathrm{GMR}} = (R_{AP} - R_P)/R_P \tag{10.26}$$

Substitution gives:

$$F_{\mathrm{GMR}} = (1/4)\,(R_\uparrow + R_\downarrow)^2 / R_\uparrow R_\downarrow \tag{10.27}$$

Note that the larger the difference between the two spin resistances, the greater is F_{GMR}. Improving the conductance of the FM layer, which is dominated by up-spin

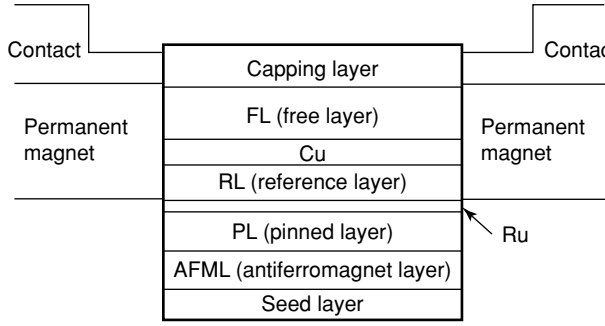

FIGURE 10.6 Schematic of cross section of a CIP spin-valve GMR sensor. The ruthenium (Ru) and copper (Cu) spacer layers are in between the PL and RL, and RL and FL, respectively. Electrical contacts are made to the biasing permanent magnets. Not shown are electrically isolated conducting shields (such as will be discussed in Chapter 13) that are above and below the sensor [19].

electrons, can be done by reducing the number of impurities or increasing the material grain size, thereby reducing $R_{\uparrow}$ more than $R_{\downarrow}$, thereby increasing F_{GMR}.

Figure 10.6 shows a way to use these two spin resistances to make a CIP (current-in-plane) spin valve GMR sensor. The purpose of the seed layer is to set the correct crystal texture and to optimize grain size. The antiferromagnet layer (AFML) helps keep the magnetization of the pinned layer (PL) in a fixed direction. The thin ruthenium (Ru) layer promotes a strong interaction between the PL and the reference layer (RL), keeping them AP. A typical thickness of the Ru layer is 0.9 nm. The thickness of the PL and RL layers is adjusted so that they have nearly equal magnetic moment (total magnetization). This makes the net moment of the PL–Ru–RL system nearly zero, forming what is called a synthetic antiferromagnet. Thus the PL and RL do not respond to the external field to be sensed, nor do they disturb the free layer (FL). A Cu spacer separates the RL and FL; on top of which is a capping layer typically made of TaN.

The GMR signal in Figure 10.6 is generated in the RL–Cu–FL layers. The FL magnetization direction rotates in response to the field to be sensed, changing the resistance from its minimum R_{min} for parallel FL and RL magnetizations, to its maximum for AP magnetizations. The resistance as a function of the angle θ between the FL and the RL magnetization directions is [19]:

$$R = R_{\text{min}}[1 + {}^1\!/_2 F_{\text{GMR}}(1 - \cos\theta)] \tag{10.28}$$

The FL is biased by permanent magnets in Figure 10.6 so that its magnetization is perpendicular to the RL magnetization in the absence of the external field to be sensed.

Spin valve magnetoresistive read heads such as shown in Figure 10.6 are now very popular in magnetic disk drives. The next chapter includes a discussion of other types of recording heads. It contrasts and compares them with magnetoresistive heads.

PROBLEMS

10.1 Redo Example 10.1 when the current measured is reduced to 2 mA.

10.2 Show all the steps between (P10.1.7), (P10.1.8), and (P10.1.9).

10.3 Redo Example 10.4 with the conductivity reduced to 4 S/m.

10.4 Redo Example 10.4 with the conductivity reduced to 1 S/m.

10.5 Redo Example 10.7 for the current of Example 3.2 reduced by 50%.

REFERENCES

1. Greiner RA. *Semiconductor Devices and Applications*, McGraw-Hill Book Co.; 1961, pp. 80–81.
2. Brauer JR, Ruehl JJ, MacNeal BE, Hirtenfelder F. Finite element analysis of Hall effect and magnetoresistance. *IEEE Trans Electron Devices* 1995;42:328–333.
3. Kittel Charles. *Introduction to Solid State Physics*, 3rd ed. New York: John Wiley & Sons; 1967, pp. 240–244.
4. Gauthier S. Tracking motion with multipole-magnet Hall sensing. *Motion System Design* 2012;54:34–37.
5. Simpkins A, Todorov E. Position estimation and control of compact BLDC motors based on analog Hall effect sensors. *Proceedings of the American Control Conference*, 2010, pp. 1948–1955.
6. Klaiber B, Turpin P. Sensing currents for maximum efficiency. *EE Times Magazine*, 2012, pp. 26–30.
7. Schneider PE, Horio M, Lorenz RD. Integrating GMR field detectors for high-bandwidth current sensing in power electronic modules. *IEEE Trans Ind Appl* 2012;48:1432–1439.
8. White RL. Giant magnetoresistance: a primer. *IEEE Trans Magn* 1992;28:2482–2487.
9. White RL. Giant magnetoresistance materials and their potential as read head sensors. *IEEE Trans Magn* 1994;30:346–352.
10. Takagishi M, Koi K, Yoshikawa M, Funayama T, Iwasaki H, Sahashi M. The applicability of CPP-GMR heads for magnetic recording. *IEEE Trans Magn* 2002;38:2277–2282.
11. Fukuzawa H, Yuasa H, Hashimoto S, Koi K, Iwasaki H, Takagishi M, Tanaka Y, Sahashi M. MR ratio enhancement by NOL current-confined-path structures in CPP spin valves. *IEEE Trans Magn* 2004;40:2236–2238.
12. Lei ZQ, Leung CW, Li L, Li GJ, Feng G, Castillo A, Chen PJ, Lai PT, Pong, PWT. Detection of iron-oxide magnetic nanoparticles using magnetic tunnel junction sensors with conetic alloy. *IEEE Trans Magn* 2011;47:2577–2580.
13. Moussa J, Ram-Mohan LR, Sullivan J, Zhou T, Hines DR, Solin SA. Finite element modeling of enhanced magnetoresistance in thin film semiconductors with metallic inclusions. *Phys Rev* 2001;B64:184410.
14. Moussa J, Ram-Mohan LR, Rowe ACH, Solin SA. Response of an extraordinary magnetoresistance read-head to a magnetic bit. *J Appl Phys* 2003;94:1110.
15. Solin SA. Magnetic field nanosensors. *Scientific American* 2004;291:71–77.

16. Brauer JR, Jenich MM. *Finite Element Analysis of a Magnetoresistive Head*, IEEE Magnetic Recording Conference, Minneapolis, MN, September 13–15, 1993.
17. Williams EM. *Design and Analysis of Recording Magnetoresistive Heads*, New York: Wiley-IEEE Press; 2000.
18. Cullity BD, Graham CD. *Introduction to Magnetic Materials*, 2nd ed. Hoboken, NJ: Wiley IEEE Press; 2009.
19. Heinonen OG, Singleton EW, Karr BW, Gao Z, Cho HS, Chen Y. Review of the physics of magnetoresistive readers, *IEEE Trans Magn* 2008;44:2465–2471.